Inorganic Chemistry

Article

pubs.acs.org/IC

Cation Templating and Electronic Structure Effects in Uranyl Cage Clusters Probed by the Isolation of Peroxide-Bridged Uranyl Dimers

Jie Qiu,[†] Bess Vlaisavljevich,[§] Laurent Jouffret,[†] Kevin Nguyen,[‡] Jennifer E.S. Szymanowski,[†] Laura Gagliardi,[§] and Peter C. Burns*[,†,‡]

[†]Department of Civil and Environmental Engineering and Earth Sciences and [‡]Department of Chemistry and Biochemistry, University of Notre Dame, Notre Dame, Indiana 46556, United States

[§]Department of Chemistry, Supercomputing Institute, and Chemical Theory Center, University of Minnesota, Minneapolis, Minnesota 55455, United States

Supporting Information

ABSTRACT: The self-assembly of uranyl peroxide polyhedra into a rich family of nanoscale cage clusters is thought to be favored by cation templating effects and the pliability of the intrinsically bent U−O_2−U dihedral angle. Herein, the importance of ligand and cationic effects on the U−O_2−U dihedral angle were explored by studying a family of peroxide-bridged dimers of uranyl polyhedra. Four chemically distinct peroxide-bridged uranyl dimers were isolated that contain combinations of pyridine-2,6-dicarboxylate, picolinate, acetate, and oxalate as coordinating ligands. These dimers were synthesized with a variety of counterions, resulting in the crystallographic characterization of 15 different uranyl dimer compounds containing 17 symmetrically distinct dimers. Eleven of the dimers have U−O_2−U dihedral angles in the expected range from 134.0 to 156.3°; however, six have 180° U−O_2−U dihedral angles, the first time this has been observed for peroxide-bridged uranyl dimers. The influence of crystal packing, countercation linkages, and $\pi-\pi$ stacking impact the dihedral angle. Density functional theory calculations indicate that the ligand does not alter the electronic structure of these systems and that the U−O_2−U bridge is highly pliable. Less than 3 kcal·mol^{-1} is required to bend the U−O_2−U bridge from its minimum energy configuration to a dihedral angle of 180°. These results suggest that the energetic advantage of bending the U−O_2−U dihedral angle of a peroxide-bridged uranyl dimer is at most a modest factor in favor of cage cluster formation. The role of counterions in stabilizing the formation of rings of uranyl ions, and ultimately their assembly into clusters, is at least as important as the energetic advantage of a bent U−O_2−U interaction.

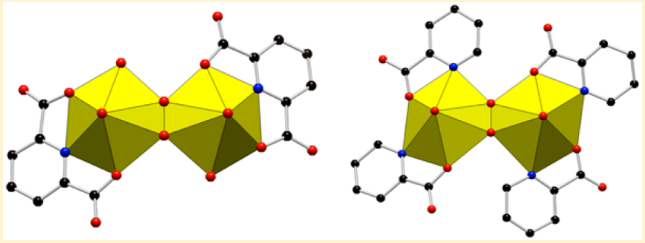

INTRODUCTION

Owing in part to their importance in the nuclear fuel cycle and in nuclear accident scenarios,[1−8] uranyl peroxide compounds have been the subject of several studies. There are only two known uranyl peroxide minerals (studtite and metastudtite), and both feature uranyl ions bridged through bidentate peroxo ligands.[7,9−12] An extensive family of uranyl peroxide nanoscale cage clusters that self-assemble in aqueous solution under ambient conditions has been characterized over the past decade.[13−16] In addition, compounds containing finite units of uranyl peroxide polyhedra have been reported that include uranyl monomers,[17−20] dimers,[21−23] a trimer,[24] a pentamer,[23] a hexamer,[23] and octomers.[25] Uranyl peroxides including chain structural units are known in studtite, $(UO_2)(O_2)(H_2O)_4$, metastudtite, $(UO_2)(O_2)(H_2O)_2$, and in two compounds synthesized using ethylenediaminetetraacetate under weak acid conditions.[25] One compound containing a uranyl peroxide sheet structural unit has been synthesized in alkaline solution and characterized.[26]

In both the minerals and the cage clusters, the U−O_2−U dihedral angles are strongly bent (Figure 1). Previous density functional theory (DFT) and wave function-based studies have indicated that a bent configuration is preferred, although the energetic advantage is relatively small.[27,28] When arranged in a ring, the bending of the U−O_2−U dihedral angle encourages curvature, as observed in the cage walls.[29] Alternatively, a series

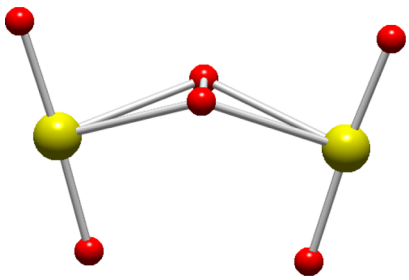

Figure 1. Peroxide-bridged uranyl dimer with a bent U−O_2−U dihedral angle. O and U atoms are shown in red and yellow, respectively.

Received: February 2, 2015
Published: April 13, 2015

DOI: 10.1021/acs.inorgchem.5b00248
Inorg. Chem. 2015, 54, 4445−4455

of U−O_2−U groups can link to form a chainlike structure as found in studtite as well as two cage clusters.[8]

In general, the self-assembly of uranyl peroxide cage clusters in aqueous solution is rapid,[30,31] and isolation of the building units as discrete entities is rare.[29] All examples of uranyl ions bridged through a bidentate peroxide group reported to date have strongly bent U−O_2−U dihedral angles, but most of these are in cage clusters where a bent configuration is mandatory. Our ongoing effort to isolate peroxo-bridged dimers of uranyl polyhedra provided the examples detailed herein. In each case, the tendency to form clusters was interrupted by coordinating the uranyl ion with combinations of pyridine-2,6-dicarboxylate, picolinate, acetate, or oxalate to form four distinct dimers (Figure 2). The inclusion of various counterions to achieve

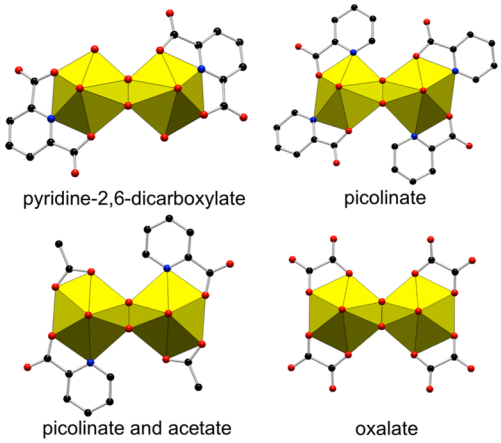

Figure 2. Polyhedral representations of the four uranyl peroxide dimers labeled by the predominate ligand type. Uranyl polyhedra are shown in yellow, O atoms are in red, N atoms are in blue, and C atoms are in black. Hydrogen atoms are not shown.

crystallization yielded 15 distinct solids (Tables 1a−1c). Isolation of these uranyl dimers provides insight into the energetics associated with modifying the dihedral angle of the U−O_2−U bridge. As the observed dihedral angles are a consequence of electronic and crystal-packing effects, DFT calculations were performed to examine the interplay of these effects.

EXPERIMENTAL SECTION

Syntheses of Compounds. ***Caution!*** *Although the isotopically depleted uranium used in this study has a very long half-life, precautions for working with radioactive materials should be followed, and such work should only take place in appropriate facilities and be conducted by properly trained individuals.*

Reagent-grade chemicals were purchased and used as received. All but two solutions were prepared using ultrapure water. The solution of pyridine-2,6-dicarboxylic acid was prepared using methanol, and the solution of uranyl nitrate for reactions of dimers **7**−**9** was prepared by using dimethyl sulfoxide (DMSO). All reactions were one-pot in 5 mL glass vials at room temperature. Subsequent to combining the reactants the vials were covered by parafilm containing small holes to permit gradual evaporation of the solutions.

$[(UO_2)_2(O_2)(H_2O)_2(C_7H_3O_4N)_2]\cdot(Et_4N)_2\cdot(H_2O)_3$ ***(1)***. This was synthesized by combining solutions of $UO_2(NO_3)_2\cdot 6H_2O$ (0.5 M, 0.1 mL), H_2O_2 (30% (w/w), 0.1 mL), tetraethylammonium hydroxide (Et_4NOH, 40% (w/w), 0.1 mL), pyridine-2,6-dicarboxylic acid (0.1 M in methanol, 0.3 mL), and citric acid (0.5 M, 0.15 mL). The pH of the resulting clear solution was 6.1. Yellow block-shaped crystals formed, together with a fine-grained precipitate, within three weeks. The yield of crystals was >35% on the basis of uranium.

$[(UO_2)_2(O_2)(H_2O)_2(C_7H_3O_4N)_2]\cdot(Et_3NH)_2\cdot(H_2O)_2$ ***(2)***. This was synthesized by combining solutions of $UO_2(NO_3)_2\cdot 6H_2O$ (0.5 M, 0.1 mL), H_2O_2 (30%, 0.1 mL), triethylamine (Et_3N, 99.5% (w/w), 0.05 mL), pyridine-2,6-dicarboxylic acid (0.1 M in methanol, 0.6 mL), and citric acid (0.5 M, 0.15 mL), resulting in a clear solution with a pH of 6.4. Yellow block-shaped crystals in 40% yield relative to uranium formed within two weeks. Anal. Calcd for the complex $C_{26}N_4O_{18}U_2H_{46}$: C, 26.48; H, 3.90; N, 4.75. Found: C, 25.29; H, 4.56; N, 4.6%. Compound **2** was reported previously in very low yield.[21]

$[(UO_2)_2(O_2)(H_2O)_2(C_7H_3O_4N)_2]\cdot(Bu_4N)_2\cdot(H_2O)_6$ ***(3)***. This was synthesized by combining solutions of $UO_2(NO_3)_2\cdot 6H_2O$ (0.5 M, 0.1 mL), H_2O_2 (30%, 0.1 mL), tetrabutylammonium hydroxide (Bu_4NOH, 40% (w/w), 0.15 mL), pyridine-2,6-dicarboxylic acid (0.1 M in methanol, 0.5 mL), and citric acid (0.5 M, 0.05 mL). The pH of the resulting clear solution was 8.9. Large yellow crystal plates formed within two weeks in a yield of 26% on the basis of uranium. Anal. Calcd for the complex $C_{46}N_4O_{22}U_2H_{94}$: C, 36.07; H, 6.14; N, 3.66. Found: C, 35.72; H, 7.04; N, 3.61%.

$[(UO_2)_2(O_2)(H_2O)_2(C_7H_3O_4N)_2]\cdot(Me_4N)_2\cdot(H_2O)_6$ ***(4)***. This was synthesized by combining solutions of $UO_2(NO_3)_2\cdot 6H_2O$ (0.5 M, 0.1 mL), H_2O_2 (30%, 0.1 mL), tetramethylammonium hydroxide (Me_4NOH, 25% (w/w), 0.1 mL), pyridine-2,6-dicarboxylic acid (0.1 M in methanol, 0.6 mL), and tartaric acid (0.5 M, 0.15 mL), resulting in a clear solution with a pH of 6.2. Yellow block-shaped crystals formed within two weeks in a yield of 51% based on uranium. Anal. Calcd for the complex $C_{22}N_4O_{22}U_2H_{46}$: C, 22.10; H, 3.85; N, 4.69. Found: C, 21.96; H, 3.76; N, 4.65%.

$K[(UO_2)_2(O_2)(H_2O)_2(C_7H_3O_4N)_2]\cdot(Et_4N)\cdot(H_2O)_3$ ***(5)***. This was synthesized by combining solutions of $UO_2(NO_3)_2\cdot 6H_2O$ (0.5 M, 0.1 mL), H_2O_2 (30%, 0.1 mL), Et_4NOH (40%, 0.075 mL), pyridine-2,6-dicarboxylic acid (0.1 M in methanol, 0.5 mL), citric acid (0.5 M, 0.2 mL), and KCl (0.5 M, 0.05 mL). The resulting solution was clear with a pH of 4.3. Yellow flake-shaped crystals formed within 1 d with a yield of 81% on the basis of uranium. Anal. Calcd for the complex $C_{22}KN_3O_{19}U_2H_{36}$: C, 22.73; H, 3.10; N, 3.62. Found: C, 22.59; H, 3.39; N, 3.61%.

$K[(UO_2)_2(O_2)(H_2O)_2(C_7H_3O_4N)_2]\cdot(Et_3NH)\cdot(H_2O)_{10}$ ***(6)***. This was synthesized by combining solutions of $UO_2(NO_3)_2\cdot 6H_2O$ (0.5 M, 0.1 mL), H_2O_2 (30%, 0.1 mL), Et_3N (99.5%, 0.04 mL), pyridine-2,6-dicarboxylic acid (0.1 M in methanol, 0.2 mL), citric acid (0.5 M, 0.15 mL), and KCl (0.5 M, 0.1 mL). The pH of the resulting clear solution was 4.7. Yellow block-shaped crystals formed within three weeks with a yield of 40% on the basis of pyridine-2,6-dicarboxylic acid. Anal. Calcd for the complex $C_{20}KN_3O_{26}U_2H_{46}$: C, 19.06; H, 3.65; N, 3.33. Found: C, 18.80; H, 2.49; N, 3.25%.

$[(UO_2)_6(O_2)_3(H_2O)_6(C_7H_3O_4N)_6]\cdot(Me_4N)_6\cdot(H_2O)_{14}$ ***(7)***. This was synthesized by combining solutions of $UO_2(NO_3)_2\cdot 6H_2O$ (0.5 M in DMSO, 0.1 mL), H_2O_2 (30%, 0.1 mL), Me_4NOH (25%, 0.1 mL), pyridine-2,6-dicarboxylic acid (0.1 M in methanol, 0.6 mL), and tartaric acid (0.5 M, 0.15 mL), which resulted in a clear solution with a pH of 5.8. A small number of yellow block-shaped crystals of **7** formed in less than a week, although continued emersion in the mother solution resulted in dissolution of the crystals within a week.

$[(UO_2)_2(O_2)(C_6H_4O_2N)_4]\cdot(Bu_4N)_2\cdot(H_2O)_3$ ***(8)*** *and* *$[(UO_2)_2(O_2)(C_6H_4O_2N)_4]\cdot(Bu_4N)_2\cdot(H_2O)_4$* ***(9)***. These were synthesized by combining solutions of $UO_2(NO_3)_2\cdot 6H_2O$ (0.5 M in DMSO, 0.1 mL), H_2O_2 (30%, 0.1 mL), Bu_4NOH (40%, 0.15 mL), picolinic acid (0.5 M, 0.2 mL), and citric acid (0.5 M, 0.1 mL). The resulting solution was clear with a pH of 5.2. When the solutions were combined, orange block-shaped crystals of **8** formed within 1 h. Over the course of several months these were replaced by yellow block-shaped crystals of **9** in a yield of 82% on the basis of uranium. Anal. **8**, anal. calcd for the complex $C_{56}N_6O_{17}U_2H_{94}$: C, 42.03; H, 5.88; N, 5.25. Found: C, 41.33; H, 6.93; N, 5.25%. **9**, anal. calcd for the complex $C_{56}N_6O_{18}U_2H_{96}$: C, 41.57; H, 5.94; N, 5.19. Found: C, 41.19; H, 6.77; N, 5.14%.

$[(UO_2)_2(O_2)(C_6H_4O_2N)_2(C_2H_3O_2)_2]\cdot(Et_4N)_2\cdot(H_2O)_6$ ***(10)*** *and* *$[(UO_2)_2(O_2)(C_6H_4O_2N)_2(C_2H_3O_2)_2]\cdot(Et_4N)_2$* ***(11)***. These were synthe-

DOI: 10.1021/acs.inorgchem.5b00248
Inorg. Chem. 2015, 54, 4445−4455

Table 1a. Crystallographic and Structure Refinement Data for 1−5

compound	1	2	3	4	5
formula	$C_{30}N_4O_{19}U_2$	$C_{26}N_4O_{18}U_2$	$C_{46}N_4O_{22}U_2$	$C_{22}N_4O_{22}U_2$	$C_{22}KN_3O_{19}U_2$
formula weight	1196.40	1132.36	1436.56	1148.32	1125.41
space group	*Cc*	*P*2/*c*	*P*2(1)/*c*	*P*2(1)/*c*	*P*2(1)/*c*
a [Å]	8.4681(8)	20.833(4)	20.9164(15)	12.1453(12)	14.800(4)
b [Å]	42.973(4)	11.573(2)	17.7959(12)	20.9227(19)	12.455(3)
c [Å]	12.5165(13)	15.800(3)	18.9742(13)	16.5252(13)	20.330(3)
α [deg]	90	90	90	90	90
β [deg]	106.7390(10)	98.452(2)	115.2120(10)	116.108(5)	119.641(13)
γ [deg]	90	90	90	90	90
V [Å^3]	4361.7(8)	3768.2(14)	6389.9(8)	3770.8(6)	3257.1(13)
Z	4	4	4	4	4
D (calc) [g/cm^{-3}]	1.822	1.996	1.493	2.023	2.295
μ (Mo K*α*) [mm]	7.487	8.658	5.128	8.661	10.141
F(000)	2176	2048	2656	2080	2032
T [K]	100(2)	100(2)	100(2)	100(2)	100(2)
λ (Mo K*α*) [Å]	0.710 73	0.710 73	0.710 73	0.710 73	0.710 73
2*θ* (min, max) [deg]	0.95, 27.51	0.99, 27.54	1.08, 27.50	1.68, 27.70	1.58, 27.50
index range (*h*, *k*, *l*)	−10:10, −55:55, −16:16	−27:27, −14:15, −20:20	−27:26, −23:23, −24:24	−15:15, −26:27, −21:21	−19:19, −16:16, −26:26
total reflections	25 724	43 833	74 684	43 852	37 362
N_{ref}, N_{par}	9846, 466	8657, 451	14 624, 676	8711, 451	7456, 424
R(int)	0.0518	0.0345	0.0331	0.0382	0.0417
R_1 ($I > 2\sigma(I)$)	0.0428	0.0275	0.0437	0.0275	0.0290
R_1 (all data)	0.0506	0.0349	0.0529	0.0396	0.0468
wR_2 ($I > 2\sigma(I)$)	0.1013	0.0731	0.1358	0.0673	0.0722
wR_2 (all data)	0.1080	0.0769	0.1435	0.0722	0.0800
S	1.039	1.040	1.081	1.035	1.033

Table 1b. Crystallographic and Structure Refinement Data for 6−10

compound	6	7	8	9	10
formula	$C_{20}K_1N_3O_{26}U_2$	$C_{66}N_{12}O_{62}U_6$	$C_{56}N_6O_{17}U_2$	$C_{56}N_6O_{18}U_2$	$C_{32}N_4O_{20}U_2$
formula weight	1213.39	3380.96	1504.68	1520.68	1236.42
space group	*P*2(1)/*c*	$P\bar{1}$	$P\bar{1}$	$P\bar{1}$	$P\bar{1}$
a [Å]	22.961(4)	12.1598(11)	18.002(2)	10.8787(11)	13.089(3)
b [Å]	6.9967(11)	12.4557(11)	18.999(3)	13.0194(13)	13.526(3)
c [Å]	25.851(4)	18.0833(16)	19.284(3)	13.0326(13)	14.194(3)
α [deg]	90	90.9440(10)	88.108(2)	73.4800(10)	79.368(2)
β [deg]	110.903(2)	97.8460(10)	89.618(2)	71.4420(10)	81.627(3)
γ [deg]	90	104.4100(10)	77.286(2)	70.9320(10)	84.113(3)
V [Å^3]	3879.7(10)	2624.2(4)	6430.3(15)	1620.0(3)	2436.2(8)
Z	4	1	4	1	2
D (calc) [g/cm^{-3}]	2.077	2.139	1.554	1.559	1.685
μ (Mo K*α*) [mm]	8.535	9.329	5.096	5.058	6.707
F(000)	2208	1528	2792	706	1128
T [K]	100(2)	100(2)	100(2)	100(2)	100(2)
λ (Mo K*α*) [Å]	0.710 73	0.710 73	0.710 73	0.710 73	0.710 73
2*θ* (min, max) [deg]	0.95, 27.5	1.14, 27.44	1.06, 25.23	1.68, 27.48	1.47, 26.84
index range (*h*, *k*, *l*)	−29:29, −9:9, −33:33	−15:15, −16:16, −23:23	−21:21, −22:22, −23:23	−14:14, −16:16, −16:16	−16:16, −17:18, −18:18
total reflections	44 445	31 300	64 408	19 344	28 019
N_{ref}, N_{par}	8881, 464	11 875, 658	23 031, 1459	7346, 370	10 398, 523
R(int)	0.0275	0.0281	0.0981	0.0232	0.0604
R_1 ($I > 2\sigma(I)$)	0.0356	0.0271	0.0714	0.0264	0.0602
R_1(all data)	0.0402	0.0324	0.1537	0.0293	0.0867
wR_2 ($I > 2\sigma(I)$)	0.0829	0.0699	0.1529	0.0725	0.1633
wR_2 (all data)	0.0850	0.0733	0.1875	0.0744	0.1795
S	1.124	1.024	1.018	0.903	1.077

DOI: 10.1021/acs.inorgchem.5b00248
Inorg. Chem. 2015, 54, 4445−4455

Table 1c. Crystallographic and Structure Refinement Data for 11−15

compound	11	12	13	14	15
formula	$C_{32}N_4O_{14}U_2$	$C_8K_6O_{26}U_2$	$C_8Na_6O_{28}U_2$	$C_4Rb_3O_{16}U_1$	$C_4Cs_3O_{16}U_1$
formula weight	1140.42	1222.74	1158.08	798.48	940.80
space group	$P2(1)/c$	$P2(1)/c$	$P2(1)/c$	$P\bar{1}$	$P\bar{1}$
a [Å]	14.069(2)	17.392(4)	6.7371(13)	7.6447(16)	7.8794(16)
b [Å]	10.0359(17)	12.102(3)	12.337(2)	10.189(2)	10.450(2)
c [Å]	16.953(2)	13.962(3)	16.243(3)	10.664(2)	11.106(2)
α [deg]	90	90	90	108.322(2)	109.505(2)
β [deg]	124.363(10)	111.526(4)	113.554(6)	95.351(2)	93.175(2)
γ [deg]	90	9	90	97.444(2)	97.678(3)
V [Å^3]	1975.9(5)	2733.7(11)	1237.6(4)	773.9(3)	849.4(3)
Z	2	4	2	2	2
D (calc) [g/cm^{-3}]	1.917	2.971	3.108	3.427	3.679
μ (Mo Kα) [mm]	8.249	12.852	13.300	19.943	15.966
F(000)	1032	2216	1044	710	818
T [K]	100(2)	100(2)	100(2)	100(2)	100(2)
λ (Mo Kα) [Å]	0.710 73	0.710 73	0.710 73	0.710 73	0.710 73
2θ (min, max) [deg]	2	1.26, 27.57	2.14, 27.49	2.03, 27.57	1.96, 27.50
index range (h, k, l)	−18:18, −13:12, −21:22	−22:22, −15:15, −18:18	−8:8, −16:16, −20:20	−9:9, −12:13, −13:13	−10:9, −13:13, −14:14
total reflections	21 908	31 265	14 432	6918	7610
N_{ref}, N_{par}	4723, 235	6296, 379	2842, 199	3472, 217	3811, 212
R(int)	0.0965	0.0329	0.0605	0.0527	0.0680
R_1 ($I > 2\sigma(I)$)	0.0419	0.0214	0.0254	0.0530	0.0561
R_1 (all data)	0.0807	0.0302	0.0301	0.0613	0.0836
wR_2 ($I > 2\sigma(I)$)	0.0826	0.0526	0.0612	0.1248	0.1196
wR_2 (all data)	0.0958	0.0563	0.0637	0.1308	0.1327
S	0.994	0.998	1.072	1.099	1.074

sized by combining solutions of $UO_2(NO_3)_2{\cdot}6H_2O$ (0.5 M, 0.1 mL), H_2O_2 (30%, 0.1 mL), Et_4NOH (40%, 0.1 mL), picolinic acid (0.5 M, 0.1 mL), and acetic acid (17 M, 0.05 mL), which gave a clear solution with a pH of 4.0. Tabular crystals of **10** and small yellow flake-shaped crystals of **11** formed together within one month, with a combined yield of >80% on the basis of uranium.

*$K_6[(UO_2)_2(O_2)(C_2O_4)_4]{\cdot}(H_2O)_4$ (**12**).* This was synthesized by combining solutions of $UO_2(NO_3)_2{\cdot}6H_2O$ (0.5 M, 0.1 mL), H_2O_2 (30%, 0.1 mL), KOH (2.5 M, 0.15 mL), and oxalic acid (0.5 M, 0.275 mL). This resulted in a cloudy solution that was centrifuged for 3 min at a rate of 10 000 rcf. The resulting top clear solution was transferred to a new vial, and its pH was measured at 5.5. Orange block-shaped crystals of **12** formed within 1 day with a yield of 48% on the basis of uranium. Anal. Calcd for the complex $C_8K_6O_{26}U_2H_8$: C, 7.80; H, 0.65. Found: C, 7.26; H, 0.66%. A different synthesis method for **12**, as well as it structure, was previously reported by our group.[29]

*$Na_6[(UO_2)_2(O_2)(C_2O_4)_4]{\cdot}(H_2O)_6$ (**13**).* This was synthesized by combining solutions of $UO_2(NO_3)_2{\cdot}6H_2O$ (0.5 M, 0.1 mL), H_2O_2 (30%, 0.1 mL), NaOH (2.5 M, 0.15 mL), and oxalic acid (0.5 M, 0.35 mL), which gave a clear solution with a pH of 4.7. Orange block-shaped crystals formed within three weeks with a yield of 20% on the basis of uranium. Anal. Calcd for the complex $C_8Na_6O_{28}U_2H_{12}$: C, 8.20; H, 1.02. Found: C, 8.93; H, 1.09%.

*$Rb_6[(UO_2)_2(O_2)(C_2O_4)_4]{\cdot}(H_2O_2)_3{\cdot}(H_2O)_4$ (**14**).* This was synthesized by combining solutions of $UO_2(NO_3)_2{\cdot}6H_2O$ (0.5 M, 0.1 mL), H_2O_2 (30%, 0.1 mL), RbOH (50% (w/w), 0.1 mL), and oxalic acid (0.5 M, 1.1 mL). This resulted in a cloudy solution that was centrifuged for 3 min at a rate of 10 000 rcf. The resulting top clear solution was transferred to a new vial, and its pH was measured at 4.9. Yellow needle-shaped crystals formed within 3 h in a yield of 31% on the basis of uranium. Anal. Calcd for the complex $C_8Rb_6O_{32}U_2H_{14}$: C, 5.96; H, 0.87. Found: C, 5.51; H, 0.80%.

*$Cs_6[(UO_2)_2(O_2)(C_2O_4)_4]{\cdot}(H_2O_2)_3{\cdot}(H_2O)_4$ (**15**).* This was synthesized by combining solutions of $UO_2(NO_3)_2{\cdot}6H_2O$ (0.5 M, 0.1 mL), H_2O_2 (30%, 0.1 mL), CsOH (50% (w/w), 0.1 mL), and oxalic acid (0.5 M, 0.8 mL). The resulting solution was cloudy and was centrifuged for 3 min at a rate of 10 000 rcf. The top clear solution was transferred to a new vial, and its measured pH was 4.6. Yellow needle-shaped crystals formed within one week in a yield of 15% on the basis of uranium. Anal. Calcd for the complex $C_8Cs_6O_{32}U_2H_{14}$: C, 5.1; H, 0.73. Found: C, 5.44; H, 0.64%.

Single-Crystal X-ray Diffraction. A suitable single crystal of each compound was selected under an optical microscope and was subsequently mounted on a cryoloop using mineral oil. It was aligned on the goniometer of a Bruker APEX II three-circle diffractometer using graphite monochromated Mo Kα X-radiation provided by a conventional sealed tube with flowing N_2 gas at 100 K to cool the crystal. The Bruker APEXII software was used for the determination of the unit cells and collection of a sphere of data using frame widths of 0.5° in ω and an exposure time per frame of 40 s. The APEXII software was used for data integration and corrections for Lorentz, polarization, and background effects. SADABS[32] was used for semiempirical absorption corrections, and SHELXTL[33] was used for structure solutions and refinements. As is typical for uranyl compounds, the H atoms were not located in the structures. Otherwise, the solution and refinement of each structure was straightforward, and the final refinement cycles included anisotropic displacement parameters for all non-C cations, and most C and O atoms. Crystallographic information is summarized in Tables 1a−1c, with further details and CIF files in the Supporting Information.

DOI: 10.1021/acs.inorgchem.5b00248
Inorg. Chem. 2015, 54, 4445−4455

C, H, and N Analysis. Crystals were isolated and rinsed with water, and they were analyzed using a Costech elemental analyzer (ECS 4010).

Spectroscopic Characterization. Infrared spectra of single crystals of each compound were collected from 600 to 4000 cm^{-1} using a SensIR technology IlluminatIR FT-IR microspectrometer. To do this, crystals were placed on glass slides and crushed using a diamond attenuated total reflectance (ATR) microscope objective.

Raman spectra for single crystals of each compound were collected using a Bruker Sentinel system linked via fiber optics to a video-assisted Raman probe equipped with a 785 nm 400 mW laser and a high-sensitivity, TE-cooled, 1024 × 255 CCD array. The spectra were collected for 5 s with five signal accumulations over the range of 80–3200 cm^{-1}. Raman spectra for reaction solutions were collected using the same system but with 15 s used for each of three signal accumulations in the range of 80–3200 cm^{-1}.

Density Functional Theory. Geometry optimizations were performed with density functional theory using the Perdew–Burke–Ernzerhof (PBE)[34] and B97-D functionals[35] with the def-TZVP basis sets[36] for all atoms as implemented in the Turbomole 5.10.2 package.[37] The corresponding def-ECP was used for U,[38] and the resolution of the identity approximation[39,40] was introduced for the Coulomb integrals. These systems contain aromatic groups in close proximity with large organic counterions; therefore, dispersion effects play an important role. B97-D is a semiempirical dispersion corrected functional and Grimme's D2 parameters were employed.[35] Vibrational frequencies were computed using the harmonic approximation to confirm that the structures were minima. Topological analysis of the electron density was performed using Bader's atoms in molecular theory[41,42] as implemented in the software package AIMAll.[43]

Results. Synthesis reactions in aqueous solutions yielded compounds **1**–**15** that were characterized with X-ray diffraction that revealed four chemically distinct peroxide-bridged uranyl dimers (see Figure 2 and Tables 1a–1c). In each case, the uranyl ion coordination polyhedra are completed by various organic ligands that tend to prevent the dimers from further assembling into cage clusters. In some cases, a given dimer was crystallized using different counterions, further extending our ability to assess the impact of crystal packing and steric effects on the $U–O_2–U$ dihedral angles.

Syntheses and Spectroscopy of Solutions. Compounds **1**–**15** were synthesized in one-pot reactions at room temperature that combined uranyl ions and peroxide, as well as various other ligands and counterions. Uranyl peroxide cage clusters are generally the dominant species where uranyl and peroxide are combined under alkaline conditions.[15] Previously, three uranyl peroxide dimers containing the $U–O_2–U$ bridge have been isolated: $[HNEt_3]_2[(UO_2)_2L_2O_2(H_2O)_2]\cdot 2H_2O$ (L = pyridine-2,6-dicarboxylate),[21] $Na_2Rb_4(UO_2)_2(O_2)_5(H_2O)_{14}$,[22] and $K_6(H_2O)_4[(UO_2)_2(O_2)(C_2O_4)_4]$.[23] We extended the family of uranyl dimer compounds by choosing organic ligands and controlling experimental conditions to avoid nanoclusters. Pyridine-2,6-dicarboxylate is particularly useful in this regard, as it binds uranyl in a tridentate arrangement that precludes the coordination of more than one bidentate peroxide ligand,[21,44,45] and therefore the formation of cage clusters.[46] Picolinate, oxalate, and acetate were used in different combinations to isolate additional uranyl dimers, although success is more dependent on ideal reactant ratios, as these ligands coordinate uranyl in a bidentate fashion, leaving the possibility of cage cluster assembly. We have previously reported this phenomenon in the case of uranyl peroxide oxalates.[29]

Raman spectra (Figures 3–5) and small-angle X-ray scattering (SAXS) profiles (Supporting Information, Figure S14) were used to characterize reaction solutions prior to crystal growth. Raman modes for precursor solutions of **1**–**7** (Figure 3) around 820 and 837 cm^{-1} are assigned as the $(UO_2)^{2+}$ stretch and the O–O stretch of peroxide coordinated to uranyl, respectively.[47] Bands at ∼1020 cm^{-1} are assigned as the ring-breathing mode of coordinated pyridine.[48,49] These spectra demonstrate that uranyl peroxide complexes containing pyridine-2,6-dicarboxylate are present in the reaction solutions. For the Raman spectrum of the precursor solution of **8** and **9** (Figure 4),

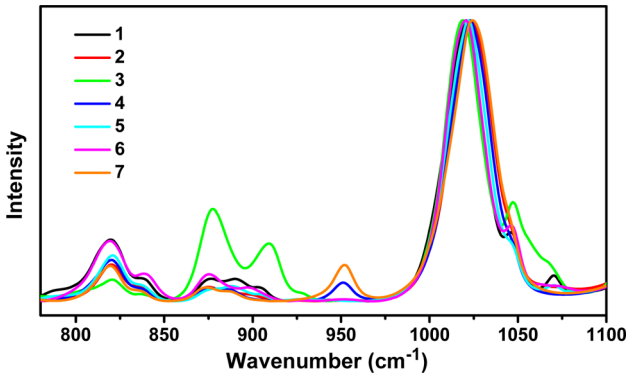

Figure 3. 780–1100 cm^{-1} region of the Raman spectra of reaction solutions that yielded **1**–**7**.

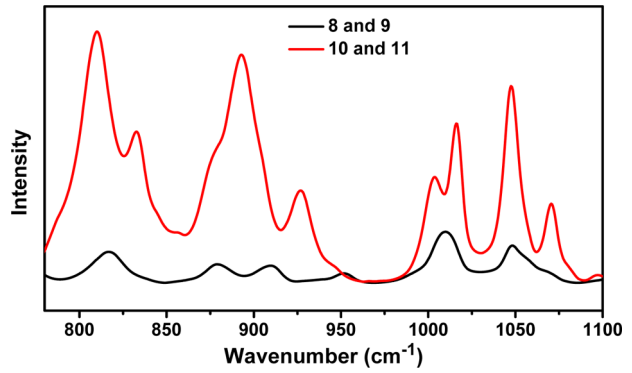

Figure 4. 750–950 cm^{-1} region of the Raman spectra of reaction solutions that yielded **8**–**11**.

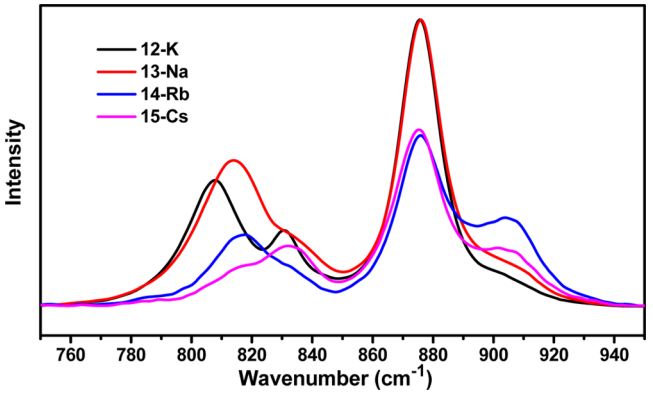

Figure 5. 300–1800 cm^{-1} region of the Raman spectra of reaction solutions of that yielded **12**–**15**.

bands at 810 and 833 cm^{-1} are assigned as for **1**–**7**.[47] Bands at ∼1003 and ∼1016 cm^{-1} are assigned as the ring-breathing modes of free and coordinated pyridine, respectively.[48,49] The spectrum indicates the formation of uranyl–peroxide complexes containing picolinate in solution. In the Raman spectrum of the precursor solution for **10** and **11** (Figure 4), bands corresponding to the $(UO_2)^{2+}$ stretching mode and the O–O stretching mode of peroxide coordinated to the uranyl ion appear to overlap at ∼818 cm^{-1}, and the band at ∼1010 cm^{-1} is assigned to the ring-breathing modes of free and coordinated pyridine.[48,49] For Raman spectra corresponding to **12**–**15** solutions (Figure 5), the $(UO_2)^{2+}$ stretches are assigned to bands centered in the region of 808–818 cm^{-1}, and those at ∼832 and 876 cm^{-1} are assigned as the stretches of peroxide coordinated to the uranyl ion and free peroxide, respectively.[47,50] Bands at ∼905 cm^{-1} are assigned to the C–C stretching mode of oxalate.[51] The SAXS profiles collected for

DOI: 10.1021/acs.inorgchem.5b00248
Inorg. Chem. 2015, 54, 4445–4455

reaction solutions prior to crystal formation do not indicate the presence of significant quantities of nanoscale cage clusters (Figure S14), which previous studies have shown are readily detectable using this method.[16,30,31]

Structure Descriptions. The structures of **1**−**15** contain a total of four chemically distinct dimers of uranyl polyhedra (see Figure 2), the charges of which are balanced by combinations of Na^+, K^+, Rb^+, Cs^+, triethylammonium (Et_3NH^+), tetramethylammonium (Me_4N^+), tetraethylammonium (Et_4N^+), and tetrabutylammonium cations (Bu_4N^+). Among all of these structures, the U≡O bond lengths range from 1.723(9) to 1.812(9) Å, and the O≡U≡O bond angles are slightly bent, ranging from 174.7(3) to 178.7(4)°, as is typical for uranyl compounds.[52] The role of the peroxo ligands is limited to bridging two uranyl ions, and the O−O bond lengths range from 1.403(19) to 1.486(10) Å.

All of the uranyl polyhedra in **1**−**15** are hexagonal bipyramids with the uranyl oxygen atoms at the apexes. In its equatorial plane, each bipyrimid contains a peroxide group, with the remaining positions filled by the organic ligand (either N or O donors), and, in some cases, H_2O. The equatorial U−O bond lengths range from 2.253(17) to 2.535(7) Å, whereas U−N bond lengths range from 2.567(5) to 2.759(4) Å, consistent with other uranyl complexes incorporating pyridine-2,6-dicarboxylate[21,44,45] and picolinate.[53,54] Likewise, the geometric parameters for the oxalate and acetate are consistent with literature values.[55]

The dimer of uranyl polyhedra in compounds **1**−**7** is illustrated in Figure 2, upper left. Each uranyl ion is coordinated by a bidentate peroxide, a tridentate pyridine-2,6-dicarboxylate, and a single H_2O group. Different combinations of counterions, listed in Table 2, were used for the crystallization of enantiomorphic pairs of the dimer. The chirality of the uranyl peroxide dimer arises from the bent U−O_2−U dihedral angle in seven of the eight symmetrically distinct dimers across compounds **1**−**7** (Supporting Information, Figures S7 and S8). The U−O_2−U dihedral angles in this series of compounds range from 134 to 180°, although all but one of the eight symmetrically distinct dimers includes a strongly bent dihedral angle of at least 156.3° (see Figure S8 and Table 2).

Table 2

structure number[a]	ligands	cations[b]	U−O_2−U[c] dihedral angle
1	pyridine-2,6-dicarboxylate and water	two Et_4N^+	134.0
2		two Et_3NH^+	136.0
3		two Bu_4N^+	138.6
4		two Me_4N^+	139.5
5		one K^+ and one Et_4N^+	139.9
6		one K^+ and one Et_3NH^+	156.3
7		two Me_4N^+	150.3/180.0
8	picolinate	two Bu_4N^+	150.4/153.1
9		two Bu_4N^+	180.0
10	picolinate and acetate	two Et_4N^+	154.1
11		two Et_4N^+	180.0
12	oxalate	six K^+	155.6
13		six Na^+	180.0
14		six Rb^+	180.0
15		six Cs^+	180.0

[a]Structures reported herein can be divided into four groups by the nature of the equatorial ligands. Each dimer has been crystallized with at least two cations. Therefore a number is assigned to each structure for clarity. [b]Me_4N^+ = tetramethylammonium, Et_4N^+ = tetraethylammonium, Et_3NH^+ = triethylamine, Bu_4N^+ = tetrabutylammonium. [c]The U−O_2−U dihedral angle is reported in degrees for each case.

Compounds **8** and **9** both contain dimers of uranyl ions with picolinate in their coordination polyhedra (Figure 2, upper right). Each uranyl ion in **8** and **9** is coordinated by two bidentate picolinate ligands, each of which provide an O and N atom to the uranyl coordination environment, in addition to the bridging peroxide. In **8**, the dimers occur as enantiomorphic pairs, and the U−O_2−U dihedral angles of the two symmetrically distinct dimers are 150.4 and 153.1° (Supporting Information, Figure S9). In **9**, the U−O_2−U dihedral angle is 180°, and therefore there is no chirality (Supporting Information, Figure S10). Both structures include tetrabutylammonium cations, and both crystallize in space group $P\bar{1}$. In **8**, there are four symmetrically distinct U positions, giving rise to two unique U−O_2−U dihedral angles, whereas in **9** there is a single symmetrically distinct U site. The formula units differ only in the presence of one additional interstitial H_2O group in **9**. Crystals of **8** formed first in solution, but they were replaced by **9** after several months. Note that during crystallization the conditions were dynamic as the solutions slowly evaporated, and the replacement of **8** by **9** would not necessarily occur under static conditions.

Compounds **10** and **11** contain uranyl dimers in which each uranyl ion is coordinated by bidentate picolinate and acetate ligands in addition to the peroxide group (Figure 2, lower left). Although the counter cations are tetraethylammonium in both cases, the U−O_2−U dihedral angle in **10** is 154.1°, and the dimers occur as enantiomorphic pairs (Supporting Information, Figure S11), but in **11** the dimer has a dihedral angle of 180° (Supporting Information, Figure S12). Compounds **10** and **11** crystallized from the same solution, and both were present at the time of harvesting. Compound **10** crystallizes in $P\bar{1}$ and contains six H_2O molecules per formula unit. Compound **11** crystallized in $P2_1/c$ and is compositionally identical to **10** except that it is anhydrous. Figure 6 compares the packing of peroxide-bridged uranyl dimers in **10** and **11**. Tetraethylammonium cations are located between the dimers in each structure, but H_2O is only present in **10**.

All of the dimers of uranyl ions in compounds **12** to **15** contain uranyl ions that are each coordinated by two bidenate "side-on" oxalate groups as well as the bidentate peroxide group (see Figure 2, lower right). The charge of this dimer is −6 and is balanced by either K^+, Na^+, Rb^+, or Cs^+ ion as indicated in Table 2. The structures also contain H_2O. When K^+ is the countercation, the U−O_2−U dihedral angle is 155.6°, while for the other three counter cations, it is 180°.

Over the 15 compounds under study, we have characterized 17 symmetrically distinct dimers of peroxide-bridged uranyl ions. The U−O_2−U dihedral angles of six of these are 180°, and the others fall in the range of 134−156.3°. We note that the anisotropic displacement parameters for the constituents of the peroxide-bridged dimers across compounds **1**−**15** are unremarkable and lack evidence for disorder or dynamic behavior. Specifically, in the cases where dimer U−O_2−U dihedral angles are 180°, there is no evidence of disorder of the bridging O atoms over positions that could equate to typical bent configurations locally. The displacement ellipsoids of the peroxide-bridged dimers of uranyl polyhedra in **12**−**15**, as well as the surrounding cations, are shown in Figure 7. Inspection of the displacement ellipsoids of the four compounds indicates that those of the uranyl dimers in **13**−**15** (180° U−O_2−U dihedral angles) are smaller than those in **12** (bent U−O_2−U dihedral angle). The counter cations in the region of the peroxide bridges exhibit normal displacement parameters, although those linked to the oxalate groups in **14** and **15** are elongated in some cases (Figure 7).

Each of the six dimers of peroxide-bridged uranyl polyhedra with U−O_2−U dihedral angles of 180° in the compounds reported here are located on an inversion center, such that the center of symmetry is on the peroxide O−O join, midway between the O atoms. The equatorial ligands as well as the counterions and H_2O groups are symmetrically distributed about these dimers. In all six cases the O−U−O uranyl ion bond angles are slightly bent, with angles in the range from 174.7 to 178.5°, increasing the separations between the uranyl ion O atoms of adjacent polyhedra. The four types of uranyl peroxide dimers encountered in this study (Figure 2) with U−O_2−U dihedral angles

DOI: 10.1021/acs.inorgchem.5b00248
Inorg. Chem. 2015, 54, 4445−4455

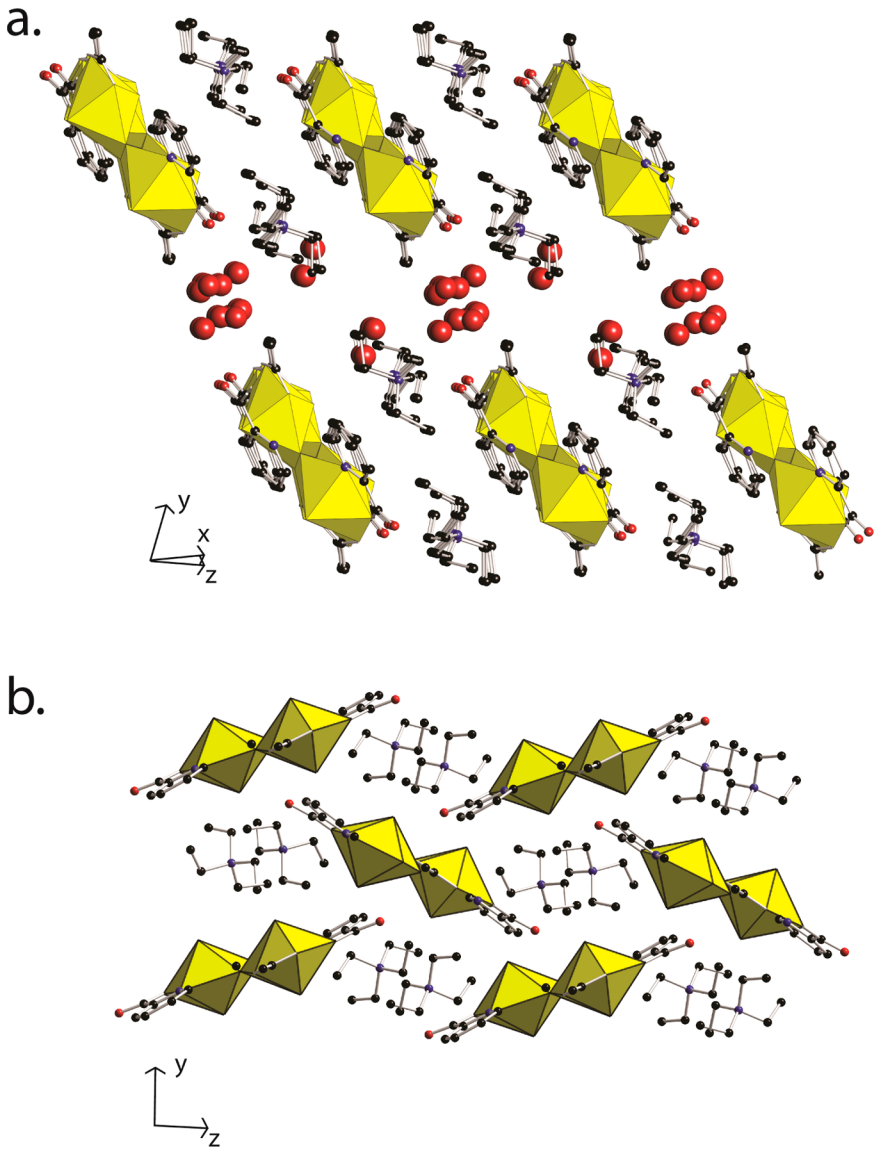

Figure 6. Mixed polyhedral and ball-and-stick representations of the packing of peroxide-bridged uranyl dimers in **10** (a) and **11** (b). Compositionally, these two compounds differ on the lack of H_2O in **11** (shown in red in **10**). Legend as in Figure 2.

of 180° are centrosymmetric, but a bent dihedral angle violates the inversion center. All of the compounds under study here except **1** crystallize in centrosymmetric space groups, but the uranyl dimers with bent dihedral angles are not located on inversion centers.

Compound **1**, in space group *Cc*, is polar, with all of the dimers of uranyl polyhedra bent in the same direction. The dimers are separated by Et_4N cations, and there are no $\pi-\pi$ interactions. In compounds **2**–**15**, the dihedral angles of uranyl dimers are bent in alternating directions, and there are $\pi-\pi$ interactions between adjacent dimers in some cases.

Ligand Effects on the Dihedral Angle. Following solution of the structures of **1**–**15**, we initially hypothesized that ligand-induced electronic effects influence the U–O_2–U dihedral angles of peroxide-bridged uranyl dimers, prompting us to study the electronic structure of these species by DFT. Although calculations were performed using both of the PBE and B97-D functionals, the following discussion focuses on the results from the B-97D calculations. Our objective was to distinguish the roles of intramolecular versus intermolecular interactions in producing the breadth of dihedral angles observed experimentally. Therefore, we first optimized the geometries of each dimer in solvent, without counter cations present. Doing this provides the minimum energy configuration of the dimer including only intramolecular interactions. The calculated bond distances and angles, with the exception of the U≡O distances and the U–O_2–U dihedral angles, are in good agreement with the experiment-derived values for all of the structures (see Supporting Information for details). U≡O distances are slightly shorter in the experimentally derived structures, which is often attributed to packing effects in the solid state. The U–O_2–U dihedral angles for the optimized structures of the four dimers shown in Figure 2, containing pyridine-2,6-dicarboxylate, picolinate, picolinate/acetate, and oxalate, respectively, are 130.5°, 144.4°, 159.7°, and 142.7° (Table 3), indicating at most a modest ligand effect on the dihedral angle. Furthermore, the different ligands did not impact the electronic structure of the U–O_2–U bridging group. In all cases, the highest occupied molecular orbitals correspond to either peroxide bonding orbitals or ligand bonding orbitals, and the lowest unoccupied orbitals are the uranium 5f orbitals, consistent with previous studies of uranyl peroxide species.[27,28] A topological analysis of the electron density using the atoms in molecules (AIM) approach confirmed that the nature of the bonding in the U–O_2–U unit remains unchanged across the series of dimers explored (see Supporting Information for details). Specifically, we did not observe a change in the electronic structure when we varied the uranyl-coordinating equatorial ligand; therefore, it is unlikely that the observed changes in the U–O_2–U dihedral angle are a direct result of the ligand.

DOI: 10.1021/acs.inorgchem.5b00248
Inorg. Chem. 2015, 54, 4445–4455

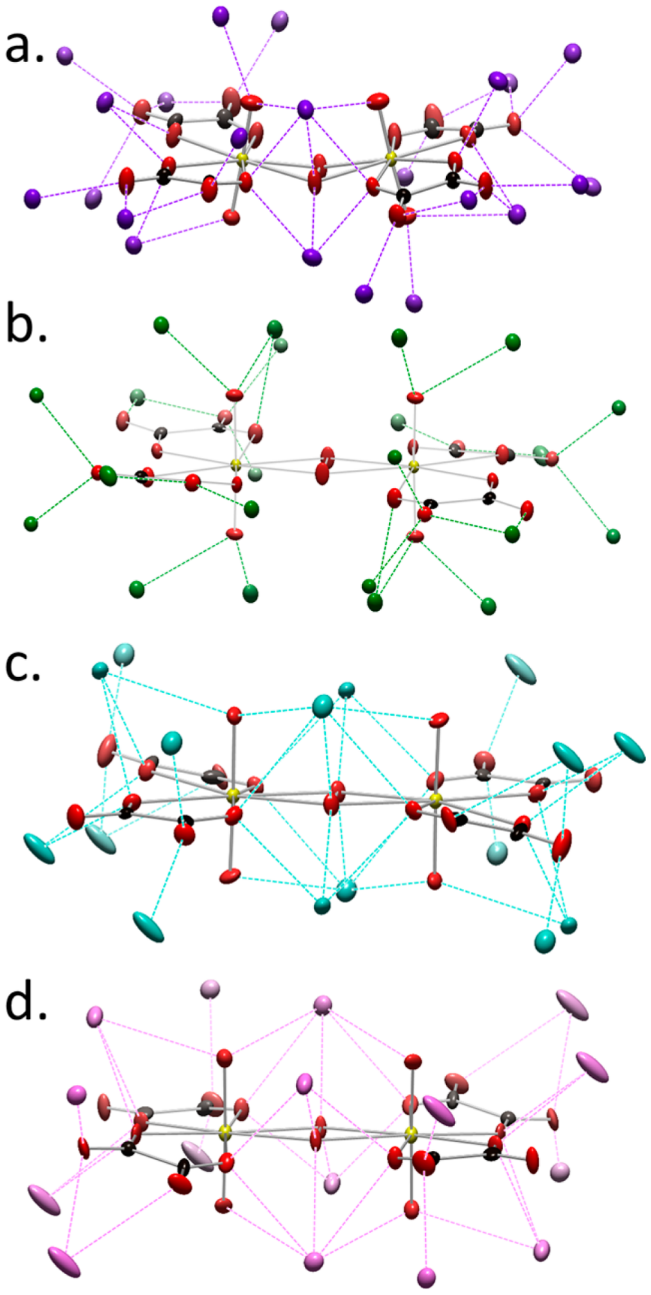

Figure 7. Displacement-ellipsoid representations of the peroxide-bridged uranyl dimers **12** (a), **13** (b), **14** (c), and **15** (d) including the distribution of counter cations and showing their bonds to the dimer. Ellipsoids are drawn at the 50% probability level. Uranyl ions are shown in yellow, O atoms in red, C atoms in black, K^+ ions in violet, Na^+ ions in green, Rb^+ ions in turquoise, and Cs^+ ions in pink.

The U−O_2−U dihedral angle in peroxide-bridged uranyl dimers is highly pliable according to previous[27,28] and current computational studies. We performed a molecular dynamics study of the $[(UO_2)_2O_2]^{2+}$ dimer in aqueous solution and observed that the dimer is so pliable that it readily inverts.[56] Over 5 ns, the average U−O_2−U angle was 171°, but it ranged from ∼160° to 180°. Figure 8 shows the potential energy surface (PES) along this bending motion for the four ligands. The dihedral angle was varied in 5° increments from 120° to 180°, and a constrained geometry optimization was performed by relaxing all other parameters. The calculations indicated that less than 4 kcal·mol^{-1} is required to distort the dihedral angle over a 50° range in all cases. This is well within the energy barrier that crystal-packing effects, including counter cations and $\pi-\pi$ stacking, can overcome,[57] and these effects are discussed in detail in the following section. Additionally, the calculations predict that, when the dimers have a U−O_2−U dihedral angle of 180°, they are at most 2 kcal/mol higher in energy than the strongly bent minima, consistent with the observed refined structures. It is also interesting to note that the oxalate structure has a local minimum near 145° but is actually lower in energy at 180°, if only by 0.5 kcal/mol.

Impact of Intermolecular Interactions on the U−O_2−U Dihedral Angle. We previously studied the peroxide-bridged uranyl dimer with oxalate and noted that the U−O_2−U dihedral angle is impacted by the associated counter cations.[28] In the previous DFT study, the K^+ counterions near to the dimer were included in the calculation. The effect of changing the size of the counterion was explored, but the initial distribution of ions was fixed. We observed that the U−O_2−U dihedral angle increases as the size of the counterion becomes larger.[28] The experimentally derived geometries of the dimers presented herein not only exhibit considerable variation in dihedral angle but also in the locations of the counterions (Table 3, Figure 9). However, any direct relationship between the geometric parameters of the uranyl dimers and the counter cations is obscured by the presence of interstitial H_2O groups, in all of the cases except for **14** (the oxalate dimer with Rb^+ cations), that could also have a significant impact on the dimer structure due to the presence of an extensive network of hydrogen bonds.

Since intermolecular interactions are expected to alter the dihedral angle of uranyl peroxide species, we extended our calculations for each of the uranyl dimers by placing one counterion near the U−O_2−U group to probe its effect. When multiple counterions were used in the synthesis, two DFT optimizations were performed (the structures of the dimers were optimized with each cation separately). The resulting values for the U−O_2−U dihedral angles are shown in Table 3. By including one counterion above the uranyl oxygen atoms, the dihedral angle is induced to vary by 1 to 15° using the B97-D functional. This confirms that the presence of even a single counterion can influence the U−O_2−U dihedral angle, but does not account for the specific U−O_2−U dihedral angles of the experimental conditions.

Most notably, adding one counterion to the DFT calculations does not lead to a dihedral angle of 180° in any case we examined. We explored the effects of the counterion position and the number of counterions in more detail for the oxalate dimer. Four counterion arrangements were considered and are shown in Figure 9. Placing a single counterion either above the peroxide group or below the peroxide group alters the dihedral angle but not in a constant size-dependent manner as we previously showed. Placing a single alkali ion above the peroxide group has little effect on the angle, while placing it below only has a large effect if the ion is small enough to reside close to the peroxide group. Likewise, if four counterions are included in the DFT calculation and are placed behind each oxalate ligand, there is little effect on the U−O_2−U dihedral angle. However, if the four alkali cations are placed near the peroxide group (as was the case in our previous study), a systematic, size-dependent change in the U−O_2−U dihedral angle is predicted (the angle becomes larger as the size of the counterion is increased). These results emphasize how sensitive the dihedral angle is to intermolecular interactions, and explains why such a large range of U−O_2−U dihedral angles is observed experimentally.

Crystal-packing effects are observed via inspection of the structures of **1**−**15**. For example, in peroxide-bridged uranyl dimers incorporating pyridine-2,6-dicarboxylate and picolinate, we note the presence of $\pi-\pi$ stacking effects between adjacent dimers. Figure 10 illustrates these interactions in **8** and **9**. The aromatic rings on both sides of the dimer in **9** have $\pi-\pi$ stacking interactions with adjacent dimers, whereas only one aromatic ring on each dimer in **8** participates in $\pi-\pi$ stacking interactions. The symmetrical $\pi-\pi$ stacking in **9** may favor a 180° U−O_2−U dihedral angle, and the variation of dihedral angles in **1**−**7** may be due to combined effects of $\pi-\pi$ stacking, interstitial water, and countercation arrangements. Likewise, in **13**, the positions of interstitial water and counterions are most likely responsible for the 180° U−O_2−U dihedral angles. In addition to interstitial H_2O and counter cations, **14** and **15** contain interstitial H_2O_2 groups that form hydrogen bonds with O atoms of oxalate groups. The combined effects

DOI: 10.1021/acs.inorgchem.5b00248
Inorg. Chem. 2015, 54, 4445−4455

Table 3. U−O_2−U Dihedral Angle (deg) from Experiment-Derived and Calculated Structures

		no counterions		one counterion		
ligand	exp (deg)	PBE[a] (deg)	B97-D[a] (deg)	PBE[a] (deg)	B97-D[a] (deg)	ion type[b]
pyridine-2,6-dicarboxylate	134.0−180.0	125.3	130.5	139.1	139.3	K^+
				126.6	131.1	Et_4N^+
picolinate	150.4/180.0	145.7	144.4	145.1	142.9	Li^+
				173.9	155.8	Bu_4N^+
picolinate and acetate	154.1/180.0	139.4	159.7	142.6	146.1	Li^+
				148.6	148.6	Et_4N^+
oxalate	155.6/180.0	142.9	142.7	144.6	150.2	Li^+
				147.2	149.9	Na^+
				146.4	147.0	K^+
				151.5	167.4	Rb^+
				144.6	1502.2	Cs^+

[a]Calculated values are given both without any counterions included (dimer only) and with a single monocation added. [b]Et_4N^+ is tetraethylammonium, and Bu_4N^+ is tetrabutylammonium.

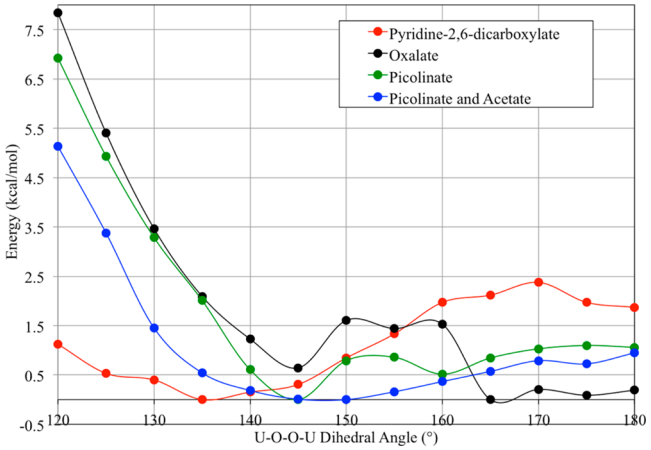

Figure 8. DFT-derived potential energy surfaces along the U−O_2−U dihedral angle for peroxide-bridged uranyl dimers incorporating different ligands within the uranyl coordination polyhedra.

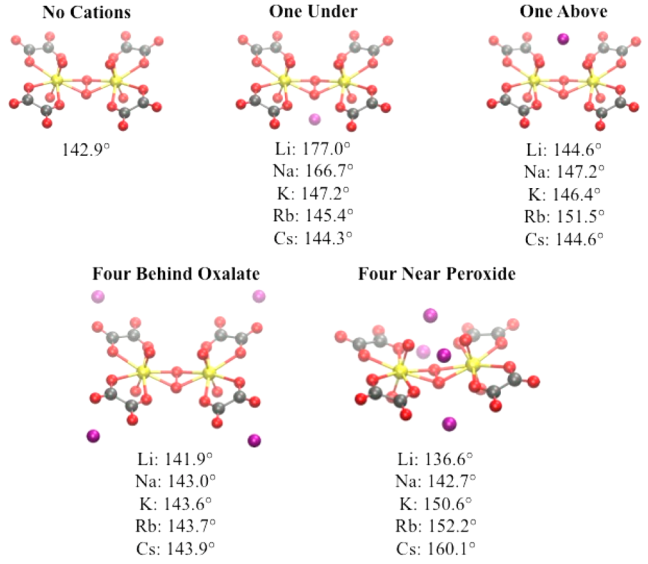

Figure 9. Oxalate dimer with zero, one, or four alkali counterions nearby. U−O_2−U dihedral angles from PBE geometry optimizations are given for each cation. Uranium is shown in yellow, oxygen in red, carbon in gray, and the alkali in purple.

of interstitial counterions, H_2O, and H_2O_2 result in 180° U−O_2−U dihedral angles.

Spectroscopy. Raman spectra collected for crystals of **1**−**15** demonstrate the presence of UO_2^{2+}, peroxide, and incorporated organic ligands (Supporting Information, Figure S1−S3). Spectra **1**−**6** contain bands centered at ∼420 and 664 cm^{-1} that are assigned as $(UO_2)^{2+}$−O [58] and $(UO_2)^{2+}$−N [59] stretches, respectively. Bands at ∼820 are assigned as $(UO_2)^{2+}$ stretches, and those at ∼834 cm^{-1} are assigned as the O−O stretch of peroxide coordinated to uranyl.[47] Bands at ∼1020 cm^{-1} are related to the ring breathing mode of coordinated pyridine.[48,49] For **8**−**11** (Supporting Information, Figure S2), bands at ∼420 and 634 cm^{-1} are assigned as $(UO_2)^{2+}$−O and $(UO_2)^{2+}$−N stretches, respectively.[58,59] Bands at ∼820 and 860 cm^{-1} correspond to $(UO_2)^{2+}$ stretches and the O−O stretch of peroxide coordinated to the uranyl ion, respectively.[47] Bands at ∼1012 and 1054 cm^{-1} correspond to the ring-breathing mode and the symmetric triangular ring deformation of the coordinated pyridine ring of the picolinate group, respectively.[48,49] The spectra of **12**− **15** (Supporting Information, Figure S3) contain a mode at ∼500 cm^{-1} that is assigned as a $(UO_2)^{2+}$−O stretch.[58] For **12**, bands at ∼812 and ∼823 cm^{-1} are assigned as $(UO_2)^{2+}$ stretches and the O−O stretch of peroxide coordinated to the uranyl ion, respectively.[47] For **13**, **14**, and **15**, a single group of bands located at ∼825, 811, and 819 cm^{-1}, respectively, presumably correspond to an overlap of $(UO_2)^{2+}$ stretch modes and the O−O stretch of peroxide coordinated to the uranyl ion.

The bands at ∼887, 876, 886, and 889 cm^{-1} for **12** to **15** are assigned to the C−C stretches of the oxalate groups.[51] The bands at ∼1443, 1461, 1458, and 1461 cm^{-1} for **12** to **15**, respectively, correspond to the C−O stretching of the carboxylate groups of oxalate.[51]

IR spectra of crystals of **1**−**15** confirmed the presence of $(UO_2)^{2+}$ and the incorporated ligands (Supporting Information, Figures S4−S6). IR spectra of **1**−**6** are very similar, with multiple bands in the region 600 to 1700 cm^{-1} (Figure S4) that are difficult to definitively assign. Those at ∼890 cm^{-1} are due to the antisymmetric stretching modes of $(UO_2)^{2+}$ ions,[60,61] those at ∼1020 cm^{-1} relate to ring-breathing vibrations of the pyridine rings of the pyridine-2,6-dicarboxylate,[62] and those at ∼1370 and 1620 cm^{-1} correspond to symmetric and asymmetric stretches of carboxylate groups of the pyridine-2,6-dicarboxylate.[44,62] Broad bands in the region of ∼2600 to 3600 cm^{-1} are due to O−H bonds.[44] For **8**−**11** (Figure S5), bands centered at ∼900 and 1005 cm^{-1} are assigned as the antisymmetric stretch of $(UO_2)^{2+}$ and the vibration of the pyridine ring of picolinate, respectively.[53] Bands at ∼1356 and 1640 cm^{-1} are due to the symmetric and asymmetric stretches of carboxylate groups from

DOI: 10.1021/acs.inorgchem.5b00248
Inorg. Chem. 2015, 54, 4445−4455

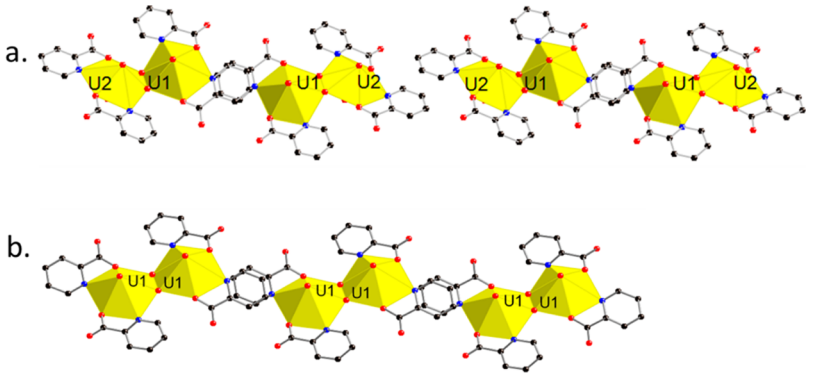

Figure 10. Mixed polyhedral and ball-and-stick representations of the peroxide-bridged uranyl dimers in **8** (a), and **9** (b) illustrating the $\pi-\pi$ stacking between adjacent dimers. Legend as in Figure 2

picolinate and acetate.[53] Broad bands in the region from ~2600 to 3600 cm^{-1} are due to O−H bonds.[53] For **12**−**15** (Figure S6), bands at ~885 cm^{-1} are assigned to antisymmetric stretching modes of the $(UO_2)^{2+}$ ions,[60,61] and those at ~1290, 1427, and 1640 cm^{-1} are related to the vibrational modes of the carboxylate groups of oxalate.[63] Bands in the region from ~2600 to 3600 cm^{-1} are assigned to O−H bonds.

DISCUSSION

We have previously argued, on the basis of experimental data, that the U−O_2−U dihedral angle of a peroxide-bridged dimer of uranyl ions is inherently bent, and that this fosters the curvature needed to assemble uranyl peroxide cage clusters.[28,29] This conclusion was supported by computational studies, although the energy advantage of the bent dihedral angle, relative to 180°, is rather modest.[27,28,64,65] Other groups have argued that counter cations are important in stabilizing and even templating four-, five-, and six-membered rings of uranyl ions that are essential to the formation of many, but not all, of the cage clusters.[27,64,66] Our earlier calculations demonstrated that the U−O_2−U dihedral angle can be influenced by the proximity of counter cations.[28] The current study provides additional insights into the relative importance of the electronic effects that favor a bent U−O_2−U dihedral angle versus linkages with counter cations. We report here peroxide-bridged dimers with 180° U−O_2−U dihedral angles for the first time. These results indicate that factors such as crystal packing, interactions with counter cations, and $\pi-\pi$ interactions between organic ligands are sufficient to overcome the energetic penalty of achieving 180° U−O_2−U dihedral angles.

Additionally, these results indicate that the energetic advantage of a bent U−O_2−U dihedral angle of a peroxide-bridged dimer is unlikely to be sufficient to require formation of cage clusters. The role of counter cations in stabilizing rings of four, five, or six uranyl ions, thus facilitating the formation of cage clusters like U_{60} (with a fullerene topology), is also clearly important. However, it is essential to note that not all of the reported cage clusters are based upon such rings of uranyl polyhedra. For example, we have reported cage clusters containing 22 and 28 uranyl ions that consist of belts of peroxide-bridged uranyl ions, with the peroxide coordinating the uranyl ions in a trans arrangement, that contain none of the typical rings of uranyl polyhedra.[30]

ASSOCIATED CONTENT

Supporting Information

Raman and infrared spectra, X-ray structure details including parameters, bond lengths, and bond angles, structure illustrations, bond critical point values, X-ray crystallographic data in CIF file, and computational details. This material is available free of charge via the Internet at http://pubs.acs.org.

AUTHOR INFORMATION

Corresponding Author

*E-mail: pburns@nd.edu.

Notes

The authors declare no competing financial interest.

ACKNOWLEDGMENTS

This material is based upon work supported as part of the Materials Science of Actinides Center, an Energy Frontier Research Center funded by the U.S. Department of Energy, Office of Science, Office of Basic Energy Sciences under Award No. DE-SC0001089.

REFERENCES

(1) Armstrong, C. R.; Nyman, M.; Shvareva, T.; Sigmon, G. E.; Burns, P. C.; Navrotsky, A. *Proc. Natl. Acad. Sci. U. S. A.* **2012**, *109*, 1874.
(2) Burns, P. C.; Ewing, R. C.; Navrotsky, A. *Science* **2012**, *335*, 1184.
(3) Chung, D.-Y.; Seo, H.-S.; Lee, J.-W.; Yang, H.-B.; Lee, E.-H.; Kim, K.-W. *J. Radioanal. Nucl. Chem.* **2010**, *284*, 123.
(4) Hanson, B.; McNamara, B.; Buck, E.; Friese, J.; Jenson, E.; Krupka, K.; Arey, B. *Radiochim. Acta* **2005**, *93*, 159.
(5) McNamara, B.; Buck, E.; Hanson, B. In *Scientific Basis for Nuclear Waste Management XXVI;* Finch, R. J., Bullen, D. B., Eds.; **2003**; Vol. *757*, p 401.
(6) Soderquist, C. Z.; Johnsen, A. M.; McNamara, B. K.; Hanson, B. D.; Chenault, J. W.; Carson, K. J.; Peper, S. M. *Ind. Eng. Chem. Res.* **2011**, *50*, 1813.
(7) Weck, P. F.; Kim, E.; Jove-Colon, C. F.; Sassani, D. C. *Dalton Trans.* **2012**, *41*, 9748.
(8) Wylie, E. M.; Peruski, K. M.; Weidman, J. L.; Phillip, W. A.; Burns, P. C. *ACS Appl. Mater. Interfaces* **2014**, *6*, 473.
(9) Kubatko, K. A. H.; Helean, K. B.; Navrotsky, A.; Burns, P. C. *Science* **2003**, *302*, 1191.
(10) Walshe, A.; Prussmann, T.; Vitova, T.; Baker, R. J. *Dalton Trans.* **2014**, *43*, 4400.
(11) Mallon, C.; Walshe, A.; Forster, R. J.; Keyes, T. E.; Baker, R. J. *Inorg. Chem.* **2012**, *51*, 8509.
(12) Burns, P. C.; Hughes, K. A. *Am. Mineral.* **2003**, *88*, 1165.

DOI: 10.1021/acs.inorgchem.5b00248
Inorg. Chem. 2015, 54, 4445−4455

(13) Burns, P. C.; Kubatko, K. A.; Sigmon, G.; Fryer, B. J.; Gagnon, J. E.; Antonio, M. R.; Soderholm, L. *Angew. Chem., Int. Ed.* **2005**, *44*, 2135.
(14) Nyman, M.; Burns, P. C. *Chem. Soc. Rev.* **2012**, *41*, 7354.
(15) Qiu, J.; Burns, P. C. *Chem. Rev.* **2013**, *113*, 1097.
(16) Qiu, J.; Ling, J.; Jouffret, L.; Thomas, R.; Szymanowski, J. E. S.; Burns, P. C. *Chem. Sci.* **2014**, *5*, 303.
(17) Alcock, N. W. *J. Chem. Soc. A* **1968**, 1588.
(18) Zehnder, R. A.; Peper, S. M.; Scott, B. L.; Runde, W. H. *Acta Crystallogr., Sect. C: Cryst. Struct. Commun.* **2005**, *61*, I3.
(19) Zehnder, R. A.; Batista, E. R.; Scott, B. L.; Peper, S. M.; Goff, G. S.; Runde, W. H. *Radiochim. Acta* **2008**, *96*, 575.
(20) Nyman, M.; Rodriguez, M. A.; Campana, C. F. *Inorg. Chem.* **2010**, *49*, 7748.
(21) Masci, B.; Thuery, P. *Polyhedron* **2005**, *24*, 229.
(22) Kubatko, K.-A.; Forbes, T. Z.; Klingensmith, A. L.; Burns, P. C. *Inorg. Chem.* **2007**, *46*, 3657.
(23) Sigmon, G. E.; Ling, J.; Unruh, D. K.; Moore-Shay, L.; Ward, M.; Weaver, B.; Burns, P. C. *J. Am. Chem. Soc.* **2009**, *131*, 16648.
(24) Unruh, D. K.; Burtner, A.; Burns, P. C. *Inorg. Chem.* **2009**, *48*, 2346.
(25) Qiu, J.; Ling, J.; Sieradzki, C.; Nguyen, K.; Wylie, E. M.; Szymanowski, J. E. S.; Burns, P. C. *Inorg. Chem.* **2014**, *53*, 12084−12091.
(26) Kubatko, K.-A.; Burns, P. C. *Inorg. Chem.* **2006**, *45*, 6096.
(27) Miro, P.; Pierrefixe, S.; Gicquel, M.; Gil, A.; Bo, C. *J. Am. Chem. Soc.* **2010**, *132*, 17787.
(28) Vlaisavljevich, B.; Gagliardi, L.; Burns, P. C. *J. Am. Chem. Soc.* **2010**, *132*, 14503.
(29) Sigmon, G. E.; Ling, J.; Unruh, D. K.; Moore-Shay, L.; Ward, M.; Weaver, B.; Burns, P. C. *J. Am. Chem. Soc.* **2009**, *131*, 16648.
(30) Qiu, J.; Kevin, N.; Jouffret, L.; Szymanowski, J. E. S.; Burns, P. C. *Inorg. Chem.* **2013**, *52*, 337.
(31) Qiu, J.; Ling, J.; Sui, A.; Szymanowski, J. E. S.; Simonetti, A.; Burns, P. C. *J. Am. Chem. Soc.* **2012**, *134*, 1810.
(32) Sheldrick, G. M. *SADABS*—Bruker AXS area detector scaling and adsorption, Version 2008/1; University of Gottingen: Germany, 2008.
(33) Sheldrick, G. M. *Acta Crystallogr., Sect. A: Found. Crystallogr.* **2008**, *64*, 112.
(34) Perdew, J. P.; Burke, K.; Ernzerhof, M. *Phys. Rev. Lett.* **1996**, *77*, 3865.
(35) Grimme, S. *J. Comput. Chem.* **2006**, *27*, 1787.
(36) Schafer, A.; Huber, C.; Ahlrichs, R. *J. Chem. Phys.* **1994**, *100*, 5829.
(37) Ahlrichs, R.; Bar, M.; Haser, M.; Horn, H.; Kolmel, C. *Chem. Phys. Lett.* **1989**, *162*, 165.
(38) Cao, X. Y.; Dolg, M. *J. Mol. Struct.: THEOCHEM* **2004**, *673*, 203.
(39) Eichkorn, K.; Treutler, O.; Ohm, H.; Haser, M.; Ahlrichs, R. *Chem. Phys. Lett.* **1995**, *240*, 283.
(40) Eichkorn, K.; Weigend, F.; Treutler, O.; Ahlrichs, R. *Theor. Chem. Acc.* **1997**, *97*, 119.
(41) Bader, R. F. W. *J. Phys. Chem. A* **1998**, *102*, 7314.
(42) Bader, R. F. W. *Atoms in Molecules: A Quantum Theory;* Clarendon Press: Oxford, U.K., 1990.
(43) Keith, T. A. *AIMAll;* TK Gristmill Software: Overland Park, KS, 2012. http://aim.tkgristmill.com/.
(44) Wang, J.; He, F.; Wang, X.; Tian, L.; Li, Z. *J. Coord. Chem.* **2011**, *64*, 2312.
(45) Jiang, Y. S.; Li, G. H.; Tian, Y.; Liao, Z. L.; Chen, J. S. *Inorg. Chem. Commun.* **2006**, *9*, 595.
(46) Burns, P. C. *Mineral. Mag.* **2011**, *75*, 1.
(47) Bastians, S.; Crump, G.; Griffith, W. P.; Withnall, R. *J. Raman Spectrosc.* **2004**, *35*, 726.
(48) Wu, D. Y.; Li, J. F.; Ren, B.; Tian, Z. Q. *Chem. Soc. Rev.* **2008**, *37*, 1025.
(49) Kolomenskii, A. A.; Schuessler, H. A. *Spectrochim. Acta, Part A* **2005**, *61*, 647.
(50) Venkateswaran, S. *Nature* **1931**, *127*, 406.
(51) Frost, R. L.; Locke, A.; Martens, W. N. *J. Raman Spectrosc.* **2008**, *39*, 901.
(52) Burns, P. C. *Can. Mineral.* **2005**, *43*, 1839.
(53) Novikov, S. A.; Peresypkina, E. V.; Serezhkina, L. B.; Virovets, A. V.; Serezhkin, V. N. *Russ. J. Inorg. Chem.* **2014**, *59*, 63.
(54) Severance, R. C.; Vaughn, S. A.; Smith, M. D.; zur Loye, H.-C. *Solid State Sci.* **2011**, *13*, 1344.
(55) Ling, J.; Qiu, J.; Burns, P. C. *Inorg. Chem.* **2012**, *51*, 2403.
(56) Miro, P.; Vlaisavljevich, B.; Dzubak, A. L.; Hu, S.; Burns, P. C.; Cramer, C. J.; Spezia, R.; Gagliardi, L. *J. Phys. Chem. C* **2014**, *118*, 24730.
(57) Hunter, C. A.; Sanders, J. K. M. *J. Am. Chem. Soc.* **1990**, *112*, 5525.
(58) Bradley, D. C.; Gitlitz, M. H. *Nature* **1968**, *218*, 353.
(59) Mer, A.; Obbade, S.; Rivenet, M.; Renard, C.; Abraham, F. *J. Solid State Chem.* **2012**, *185*, 180.
(60) Bullock, J. I. *J. Inorg. Nucl. Chem.* **1967**, *29*, 2257.
(61) Ling, J.; Albrecht-Schmitt, T. E. *Inorg. Chem.* **2007**, *46*, 346.
(62) Zhou, L.-Q.; Wang, F.; Tang, Z.-W.; Zhou, L.-R.; Sun, J.-T. *Spectrosc. Lett.* **2010**, *43*, 108.
(63) Fujita, J.; Nakamoto, K.; Kobayashi, M. *J. Phys. Chem.* **1957**, *61*, 1014.
(64) Miro, P.; Bo, C. *Inorg. Chem.* **2012**, *51*, 3840.
(65) Miro, P.; Ling, J.; Qiu, J.; Burns, P. C.; Gagliardi, L.; Cramer, C. J. *Inorg. Chem.* **2012**, *51*, 8784.
(66) Liao, Z. L.; Deb, T.; Nyman, M. *Inorg. Chem.* **2014**, *53*, 10506.

DOI: 10.1021/acs.inorgchem.5b00248
Inorg. Chem. 2015, 54, 4445−4455